

# Potential oscillations and S-shaped polarization curve in the continuous electro-oxidation of CO on platinum single-crystal electrodes

Marc T.M. Koper<sup>a)\*</sup>, Thomas J. Schmidt<sup>b)</sup>, Nenad M. Marković<sup>b)</sup>, Philip N. Ross<sup>b)</sup>

<sup>a)</sup>*Schuit Institute of Catalysis, Laboratory of Inorganic Chemistry and Catalysis, Eindhoven University of Technology, 5600 MB Eindhoven, The Netherlands*

<sup>b)</sup>*Materials Science Division, Lawrence Berkeley National Laboratory, University of California, Berkeley, CA 94720, USA*

## Abstract

The occurrence of an S-shaped polarization curve in a simple model for the continuous electrochemical oxidation of CO on a platinum electrode is discussed. In the model, the S-shaped polarization curve is caused by the competitive Langmuir-Hinshelwood mechanism between surface-bonded CO and OH. The reaction is studied experimentally on single-crystal platinum rotating disk electrodes in perchloric and sulfuric acid solution, and it is shown that the voltammetry is in good agreement with the model predictions. When studied under current-controlled conditions, a fast galvanodynamic scan indeed suggests the existence of the S-shaped polarization curve. At lower scan rates, however, irregularities and small-amplitude irregular fluctuations or oscillations in potential are observed. Very regular potential oscillations under current-controlled conditions are observed only on Pt(111) in sulfuric acid. The possible origin of these irregularities and oscillations is discussed in relation to the existing theories of electrochemical instabilities.

## 1. Introduction

The electrochemical oxidation of carbon monoxide has been the subject of numerous experimental investigations in the past few decades<sup>1-8</sup>. This interest stems primarily from the importance of CO poisoning of low-temperature fuel cell anodes, be it either during the oxidation of hydrogen/CO mixtures or methanol. An understanding of the mechanism of CO electrooxidation is therefore of great value for the development of CO tolerant anode electrocatalysts.

The electrochemical study of CO oxidation is usually carried out by so-called stripping voltammetry of a pre-adsorbed (sub-)monolayer of CO, or by the continuous oxidation of CO on an electrode with well-defined mass transport conditions, such as a rotating disk electrode (RDE). These studies have shown quite convincingly that CO electro-oxidation on platinum takes place through a Langmuir-Hinshelwood mechanism, by which the adsorbed CO reacts with an adsorbed oxygen-containing species to form CO<sub>2</sub>. The oxygen-containing species is generally believed to be some sort of adsorbed OH formed from the oxidative chemisorption of water. From the negative reaction order in the CO bulk concentration as observed in the continuous oxidation experiments<sup>6</sup>, it is concluded that these surface species compete for the same sites on the surface and that CO adsorption is generally stronger than OH adsorption.

The present study was motivated by our desire to model the continuous CO electro-oxidation using mean-field-type equations or Monte Carlo simulations<sup>9</sup>. As was already noted by Strasser et al.<sup>10</sup> in their modeling studies of formic acid oxidation on platinum, the simplest possible model for continuous electro-oxidation of CO on platinum, based on the widely accepted Langmuir-Hinshelwood mechanism, predicts an instability in the reaction's current-voltage characteristic. As we will show in the next section, this model exhibits a so-called S-shaped polarization curve, and is able to reproduce various features of the experimental voltammetry quite satisfactorily. However, the existence of the predicted instability is better studied by galvanostatic experiments, and such experiments have not yet been reported in the literature. We present here experimental evidence for the predicted instability and S-shaped polarization curve by carrying out the CO electrooxidation galvanostatically. Much to our surprise, however, we also observed the development of spontaneous potential oscillations. These oscillations have not been reported before in the literature, nor are they predicted by the "homogeneous" mean-field model. Also, the instability mechanism causing the oscillations does not seem to be the same for all single-crystal surfaces and electrolyte solutions. The Pt(111) surface in sulfuric acid solution stands out as a system leading to particularly regular potential oscillations during CO electro-oxidation. In this respect it is interesting to note that CO oxidation is one of the paradigms of an oscillating reaction in heterogeneous catalysis, both on single-crystals and supported catalysts<sup>11</sup>. However, we emphasize that the

mechanistic origin of the electrochemical oscillations reported here is very different from those occurring at the metal-gas interface.

In the next section, we will describe the simple model that predicts the S-shaped polarization curve during continuous CO electro-oxidation. We will then discuss the potentiodynamic and galvanodynamic experiments that were carried out to test the predictions of this model, and we will present evidence for the S-shape polarization curve observed on all three low-index Pt surfaces in both perchloric and sulfuric acid solution. The potential oscillations observed on some of the surfaces will be described and their possible instability mechanism discussed in terms of the existing theories of electrochemical instabilities<sup>12-15</sup>. Finally, we will briefly discuss the implications our results have on our present understanding of the mechanism of CO electro-oxidation on platinum.

## 2. Model

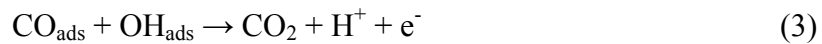
The model for CO electrooxidation considered in this paper is very similar to that originally suggested by Strasser et al.<sup>10</sup>, and based on three simple reactions. First, there is the adsorption of CO onto a free site on the platinum surface:



which we consider to be an irreversible reaction. Water can dissociate on the free sites giving adsorbed OH:



Finally, adsorbed CO and OH can react to give CO<sub>2</sub>:



As we do not allow for the desorption of CO from the platinum surface (which is known to be very slow at room temperature), we introduce a rate law for CO adsorption which assures that there always some sites available for OH adsorption:

$$v_{\text{CO,ads}} = \begin{cases} k_{\text{CO,ads}} c_{\text{CO,s}} (0.99 - \theta_{\text{CO}} - \theta_{\text{OH}}) & \text{for } \theta_{\text{CO}} + \theta_{\text{OH}} < 0.99 \\ 0 & \text{for } \theta_{\text{CO}} + \theta_{\text{OH}} > 0.99 \end{cases} \quad (4)$$

(In the model of Strasser et al.<sup>10</sup> sites are always available for OH by the introduction of a small CO desorption rate.) In this equation,  $\theta_{\text{CO}}$  and  $\theta_{\text{OH}}$  are the average coverages of CO and OH on the surface, and  $c_{\text{CO,s}}$  is the concentration of CO near the surface. Note that this means that we assume a maximum coverage of CO of 0.99. Even though the experimental coverage per surface Pt atom is lower, the actual value of this number is of no importance for the qualitative modeling. The rate law for OH formation is given by the following expression:

$$v_{\text{OH}} = k_{\text{OH,ads}} \exp(\alpha FE / RT) [\theta_{\text{OH}}^{\text{max}} (1 - \theta_{\text{CO}}) - \theta_{\text{OH}}] - k_{\text{OH,des}} \exp(-(1 - \alpha) FE / RT) \theta_{\text{OH}} \quad (5)$$

where we have assumed a Butler-Volmer-type dependence for the potential dependence of the charge-transfer reaction,  $E$  is the electrode potential and the other symbols have their usual meaning. In Eq.5 we have assumed a maximum coverage of OH,  $\theta_{\text{OH}}^{\text{max}}$ , in order to avoid a complete blocking of CO adsorption by OH at high potentials. The rate of CO oxidation is equal to:

$$v_{\text{react}} = k_r \theta_{\text{CO}} \theta_{\text{OH}} \exp(\alpha FE / RT) \quad (6)$$

These rate laws lead to the following differential equations for the time dependence of the CO and OH surface coverages:

$$\frac{d\theta_{\text{CO}}}{dt} = v_{\text{ads,CO}} - v_{\text{react}} \quad (7)$$

$$\frac{d\theta_{\text{OH}}}{dt} = \nu_{\text{OH}} - \nu_{\text{react}} \quad (8)$$

The total Faradaic current density  $j_F$  flowing is:

$$j_F = FS_{\text{tot}}(\nu_{\text{OH}} + \nu_{\text{react}}) \quad (9)$$

where  $S_{\text{tot}}$  is the total number of surface sites per  $\text{cm}^2$ . Finally, to describe the finite mass transport rate of CO from the bulk to the surface, we use a simple diffusion-layer model that describes the time dependence of the transport process quite well, and is exact under steady-state conditions<sup>16</sup>:

$$\frac{dc_{\text{CO},s}}{dt} = -\frac{2S_{\text{tot}}}{\delta} \nu_{\text{CO,ads}} + \frac{2D}{\delta^2} (c_{\text{CO,bulk}} - c_{\text{CO},s}) \quad (10)$$

where  $\delta$  is the diffusion layer thickness,  $D$  is the CO diffusion coefficient, and  $c_{\text{CO,bulk}}$  the CO bulk concentration.

The above equations can be solved by standard numerical methods. Some typical examples of cyclic voltammetric curves obtained from this model at different scan speeds and different diffusion layer thicknesses are shown in Figure 1. These curves reproduce some of the experimental curves quite well; see for instance the voltammetry of CO oxidation on Pt(100) in sulfuric acid as presented in ref. 7b, or Pt(110) in perchloric acid in Figure 4 below. We will discuss this comparison with experiment in some more detail in Section 4.

The instability is illustrated by the bold line in Figure 2, which is the steady-state current-voltage characteristic. The steady-state curve is S-shaped, and possesses a potential region between  $E_1$  and  $E_2$  in which three different steady-state current values coexist at one value of the applied electrode potential. The middle branch of the S-shaped curve is unstable and cannot be accessed by potentiostatic means, whereas the upper and lower current branches are (locally) stable. The points  $E_1$  and  $E_2$  at which two steady-state branches meet are known as saddle-node bifurcations<sup>15</sup>. The model predicts that the

existence of these multiple steady states depends strongly on mass transport conditions of the CO, i.e. on the diffusion layer thickness  $\delta$  and the CO bulk concentration  $c_{\text{CO,bulk}}$ . We find that the region of bistability between  $E_1$  and  $E_2$  (leading to the pronounced hysteresis in the voltammetry) is observed for large diffusion-layer thickness (or low rotation rate of the RDE) and low CO bulk concentration. When the mass transport of CO to the surface is sufficiently efficient, i.e. for high rotation rates and/or high CO concentrations, the S-shaped current-voltage characteristic “unfolds” into a single-valued curve with no bistability.

As mentioned, the middle branch of the S-shaped curve cannot be accessed by potentiostatic measurements. However, the branch should be accessible by galvanostatic measurements. In order to study the stability of the branch under galvanostatic conditions, we have to extend our model by an equation describing the time dependence of the electrode potential  $E$ :

$$C_d \frac{dE}{dt} = \frac{I}{A} - j_F \quad (11)$$

where  $C_d$  is the electrode’s double layer capacity,  $I$  the applied current, and  $A$  the electrode’s surface area.

Figure 3 shows the typical curves obtained when scanning the current density  $i = I/A$  galvanodynamically through the S-shaped polarization curve at different scan rates. The S-shaped curve is clearly traced by the current-controlled experiment, though with some hysteresis at finite scan rate. We emphasize that this hysteresis is of a different nature than that observed potentiodynamically (Figs.1,2), in which case it does not disappear at zero scan rate due to the bistable nature of the polarization curve under potentiostatic conditions.

### 3. Experimental

The pretreatment and assembly of the Pt(hkl) single crystals (0.283cm<sup>2</sup>, *MaTeck, Juelich, Germany*) in a RDE configuration was fully described previously<sup>17</sup>. In short,

following flame annealing in a hydrogen flame and cooling in a mild stream of Ar, the single crystal was mounted into the disk position of an insertable ring disk electrode assembly (*Pine Instruments*). Subsequently, the electrode was transferred into a thermostated standard three compartment electrochemical cell and immersed into the Ar-purged electrolyte (*Bay Gas Research Purity*) under potentiostatic or galvanostatic control at  $\approx 0.1$  V or 0.005 mA, respectively, maintained by a Bi-Potentiostat/Galvanostat (*Pine Instruments*). The measurements were carried out in either 0.1 M HClO<sub>4</sub> (*Aldrich Double Distilled Teflon Grade*) or 0.05 M H<sub>2</sub>SO<sub>4</sub> (*J.T. Baker Ultrex*), both prepared with triply pyrodistilled water. A circulating constant temperature bath (*Fischer Isotemp Circulator*) maintained the temperature of the electrolyte at 293 K  $\pm$  0.5 K. The reference electrode was a saturated calomel electrode (*SCE*) separated by a closed electrolyte bridge from the working electrode compartment in order to avoid chloride contamination. All potentials, however, refer to that of the reversible hydrogen electrode in the same electrolyte. The CO oxidation measurements were carried out in CO-saturated electrolyte under continuous CO flux (*Spectra Gases N4.5*). Before each CO oxidation experiment the electrode was held at either 0.005 V or 0.005 mA for 3 min. in order to obtain a fully CO covered surface.

#### 4. Results and Discussion

In Figure 4 we show the experimental voltammetry of CO electro-oxidation on Pt(110) in 0.1 M HClO<sub>4</sub> at different voltage scan rates (Fig.4a) and different disk rotation rates (Fig.4b), for comparison with the simulated curves in Figure 1a and 1b. It is observed that most of the qualitative features of the simulated curves are in good agreement with experiment. The width of the hysteresis decreases with decreasing scan rate but does not shrink to zero at the lowest scan rate. Also the sharp “ignition” peak observed in anodic scan behaves in accordance with the simulation: the sharpness decreases with decreasing scan rate, and with increasing disk rotation rate. This ignition peak is actually a typical “overshoot” phenomenon characteristic of scanning a system through a saddle-node bifurcation. Lowering the disk rotation rate leads to a broadening of the hysteresis in agreement with the model predictions. This illustrates the importance

of the mass transport conditions in the development of the S-shaped polarization curve. The voltammetry shown in Fig.4 for Pt(110) in HClO<sub>4</sub> is typical for all other surfaces in perchloric and sulfuric acid, including polycrystalline platinum. The only exception is Pt(111) in sulfuric acid, to be discussed further below.

We mention here that the model described in the previous section also exhibits the experimentally observed negative reaction order in CO bulk concentration<sup>6</sup>, though we do not illustrate this by a comparison of simulation and experiment. As is well known, this negative reaction order is a result of the competitive adsorption of CO and OH. The model does not describe, however, the small prewave that is consistently observed at potentials negative of the ignition potential (and discussed in some detail in ref.7). This pre-ignition oxidation wave is known to exhibit a positive reaction order in CO bulk concentration<sup>7a</sup>, suggesting that its oxidation mechanism does not involve a competitive adsorption between CO and OH. Also note the reduction peak at 0.77 V observed in the back scan at high scan rate. This peak also occurs in the model (though it is not easily discerned from Fig.1) and is due to the reduction of surface (hydr)oxides.

As mentioned in the Model section, more direct evidence for the S-shaped polarization curve can be obtained from current-controlled measurements. Figures 5-7 show some typical galvanodynamic curves we obtained for CO oxidation on Pt(110), Pt(111) and Pt(100) in HClO<sub>4</sub>. These experiments indeed strongly suggest an S-shaped polarization curve, but only at the higher scan rates, as can be seen in the back scans of Figs. 5 and 7. At lower scan rates, the obtained curve was very irregular or noisy, and most typically these irregularities occurred about a potential value which was relatively independent of the applied current (see, e.g., the 2 μA/s curves in Figs.5 and 7). When the current was halted, in certain cases small-amplitude potential oscillations could be observed, which in spite of their irregularity seemed to possess some basic periodicity. The insert in Fig.5 shows an example observed for Pt(110) in HClO<sub>4</sub>. Note that the amplitude of these oscillations was typically not larger than 30 mV. For Pt(111) in HClO<sub>4</sub> more regular oscillations could be observed during a relatively rapid scan (see Fig.6a), but these disappeared and became very irregular when the scan rate was lowered (Fig. 6b).



The electro-oxidation of CO on Pt(111) in H<sub>2</sub>SO<sub>4</sub> behaved qualitatively different from the other interfaces. The main difference in terms of voltammetry is illustrated in Figure 8. Comparing Pt(111) in HClO<sub>4</sub> and Pt(111) in H<sub>2</sub>SO<sub>4</sub>, one can clearly observe that on Pt(111) in H<sub>2</sub>SO<sub>4</sub> the CO electro-oxidation does not reach a diffusion-limited regime, as it does at the other interfaces. Rather, the current after the ignition spike decreases with increasing potential. When CO electro-oxidation on Pt(111) in H<sub>2</sub>SO<sub>4</sub> was studied under current-controlled conditions, very regular potential oscillations were observed during the current scan (Figs.9a and b), and they were sustained during a current halt (Fig.9c).

The regularity and amplitude of these oscillations suggest that they have a mechanistic origin different from the fluctuations observed at the other interfaces. We believe this is related to the region of negative differential resistance observed after the ignition spike. It is well known that such negative impedance may lead to spontaneous oscillations under the appropriate conditions<sup>12-15</sup>. We assume that this inhibition of the CO oxidation process on Pt(111) is due to the strong interaction of sulfate with this surface, competing with OH for the free surface sites. However, it is now well established that in order to observe galvanostatic potential oscillations, a so-called hidden negative impedance or differential resistance (HNDR) is required. Several qualitatively different mechanistic origins of this HDNR are now known and discussed in Ref.12. The competitive adsorption between sulfate and OH can be added to the model discussed in Section 2, leading to voltammetric behavior very similar to that shown in Fig.8, but unfortunately such a model is not able to explain the potential oscillations under galvanostatic conditions. Identification of a reasonable model for these oscillations requires a more detailed characterization of their phenomenology and parameter dependence, and this is left for future work.

The potential fluctuations or oscillations observed on the other surfaces, in particular Pt(110) in HClO<sub>4</sub> (Fig.4), do not seem to fall within one of the existing categories of electrochemical oscillators. In fact, it can be shown that potential oscillations taking place about the sandwiched branch of an S-shaped polarization curve under current-controlled conditions are extremely unlikely, as they require the electrode reactions responsible for the S-shaped polarization curve to be faster than the double-layer charging<sup>12</sup>. However,

recent theoretical considerations and simulations by Krischer et al.<sup>18,19</sup> have shown that an electrochemical system having an S-shaped polarization curve may exhibit spatio-temporal pattern formation due to the instability of the system with respect to non-homogeneous perturbations (a similar result is known for electrical devices with an S-shaped polarization curve<sup>20</sup>). This domain formation, i.e. a phase separation into low- and high-current domains, may in fact explain why at low scan rate no S-shaped curve is obtained but instead the observed potential is nearly independent of the applied current. Recent calculations by Krischer et al.<sup>18</sup> show that, as the applied current is changed, the relative size of the low- and high-current domains changes whereas the average potential is hardly affected. If this is the correct interpretation, then apparently at higher scan rates of the current this phase separation is absent or incomplete and the homogeneous S-shaped polarization curve is tracked. The fluctuations or irregular oscillations observed at low scan rate or constant current might then be due to some instability in the domain boundaries, either for some intrinsic mechanistic reason or because of imperfections in the experimental setup.

#### 4. Conclusion

In this paper we have reported the observation of an S-shaped polarization curve and spontaneous potential oscillations during the galvanostatic oxidation of CO on Pt single-crystal electrodes. It is worth noting that CO oxidation is one of the paradigms of an oscillating reaction in heterogeneous catalysis, both on single-crystals and supported catalysts<sup>11</sup>. We have shown here that oscillations may also occur in the electrochemical CO oxidation, though we must emphasize that the mechanistic origin of the electrochemical oscillations is completely different from the gas-phase oscillations. Furthermore, the existence of an S-shaped polarization curve is quite unique in electrochemistry (but see a very recent publication from the Berlin group<sup>21</sup> and ref.22), though more common in electrical devices<sup>23-25</sup>.

The observation of the S-shaped polarization curve is in agreement with the predictions of a simple model based on a Langmuir-Hinshelwood mechanism for the CO oxidation by OH. Due to the competitive adsorption of CO and OH, this model gives rise

to a strongly non-linear autocatalytic CO oxidation rate, manifesting in an S-shaped polarization curve under the appropriate mass transport conditions. This is a highly non-trivial prediction of the model and the fact that it is indeed observed experimentally, lends further credit to our mechanistic interpretation of the CO oxidation mechanism in the ignition region.

The potential irregularities and oscillations observed during a (slow) current-controlled scan are more difficult to interpret. The near independence of the (average) potential as a function of the applied current, could be interpreted as a phase separation on the electrode surface into low- and high-current domains, the relative size of which changes with overall current. The fluctuations or irregular oscillations may be due to some instability in the domain boundaries, either for some intrinsic mechanistic reason or because of imperfections in the experimental setup. Moreover, if we adhere to this phase separation picture, it does apparently not take place or is less extended during a faster scan, leading to the S-shaped polarization curve predicted by the spatially homogeneous model. Clearly, these interpretations can be only tentative and speculative without a spatio-temporal characterization of the surface and quantitative modeling.

The regular potential oscillations observed during CO oxidation on Pt(111) in H<sub>2</sub>SO<sub>4</sub> have a different origin. These appear to be “homogeneous” oscillations, and the existing data suggest that they are of the HNDR type, even though the mechanistic origin of this hidden negative differential resistance still has to be established.

#### *Acknowledgements*

We are grateful to Katharina Krischer and Peter Strasser for useful discussions. This work was supported by the Assistant Secretary for Conservation and Renewable Energy, Office of Transportation Technologies, Electric and Hybrid Propulsion Division of the U.S. Department of Energy under Contract No. DE-AC03-76SF00098 and by a grant from the Royal Netherlands Academy of Arts and Sciences.

## References

- (1) Beden, B.; Bilmes, S.; Lamy, C.; Leger, J.-M., *J.Electroanal.Chem.* **1983**, 149, 295.
- (2) Kitamura, F.; Takeda, M.; Takahashi, M.; Ito, M., *Chem.Phys.Lett.* **1987**, 143, 318.
- (3) Gasteiger, H.A.; Marković, N.M.; Ross Jr., P.N.; Cairns, E.J. *J.Phys.Chem.* **1994**, 98, 617
- (4) Feliu, J.M.; Orts, J.M.; Fernandez-Vega, A.; Aldaz, A.; Clavilier, J., *J.Electroanal.Chem.* **1990**, 296, 191
- (5) Weaver, M.J.; Chang, S.-C.; Leung, L.-W.; Jiang, X.; Rubel, M.; Szklarczyk, M.; Zurawski, D.; Wieckowski, A., *J.Electroanal.Chem.* **1992**, 327, 247.
- (6) (a) Gasteiger, H.A.; Marković, N.M.; Ross Jr., P.N., *J.Phys.Chem.* **1995**, 99, 8290  
(b) Gasteiger, H.A.; Marković, N.M.; Ross Jr., P.N., *J.Phys.Chem.* **1995**, 99, 16757.
- (7) (a) Marković, N.M.; Grgur, B.N.; Lucas, C.A.; Ross Jr., P.N., *J.Phys.Chem.B.* **1999**, 103, 487. (b) Marković, N.M.; Lucas, C.A.; Grgur, B.N.; Ross Jr., P.N., *J.Phys.Chem.B.* **1999**, 103, 9616.
- (8) Lebedeva, N.P., Koper, M.T.M., Herrero, E.; Feliu, J.M.; van Santen, R.A., *J.Electroanal.Chem.* **2000**, 487, 37
- (9) (a) Koper, M.T.M.; Jansen, A.P.J.; van Santen, R.A.; Lukkien, J.J.; Hilbers, P.A.J., *J.Chem.Phys.* **1998**, 109, 6051 (b) Saravanan, C.; Markovic, N.M., Head-Gordon, M.; Ross, P.N. *J.Chem.Phys.* **2001**, 114, 6404
- (10) Strasser, P.; Eiswirth, M.; Ertl, G., *J.Chem.Phys.* **1997**, 107, 991.
- (11) Imbihl, R.; Ertl, G., *Chem.Rev.* **1995**, 95, 697.
- (12) Strasser, P.; Eiswirth, M.; Koper, M.T.M., *J.Electroanal.Chem.* **1999**, 478, 50.
- (13) Koper, M.T.M., *Adv.Chem.Phys.* **1996**, 92, 161.
- (14) Krischer, K., in *Modern Aspects of Electrochemistry*, Bockris, J.O'M.; Conway, B.E.; White, R.E. (Eds.), Vol. 32, Plenum Press, New York, 1999, p.1.
- (15) Koper, M.T.M., *J.Chem.Soc.Faraday Trans.* **1998**, 94, 1369.
- (16) Koper, M.T.M.; Sluyters, J.H., *J.Electroanal.Chem.* **1991**, 303, 73.

- (17) Markovic, N.M.; Gasteiger, H.A.; Ross Jr., P.N., *J.Phys.Chem.* **1995**, 99, 3411.
- (18) Krischer, K. Mazouz, N.; Flätgen, G., *J.Phys.Chem.B* **2000**, 104, 7545
- (19) Mazouz, N.; Krischer, K., *J.Phys.Chem.B* **2000**, 104, 6081.
- (20) Wacker A.; Schöll, *Appl.Phys.Lett.* **1995**, 78, 7352.
- (21) Li, Y.-J.; Oslonovitch, J.; Mazouz, N.; Plenge, F.; Krischer, K.; Ertl, G., *Science* **2001**, 291, 2395.
- (22) (a) Epelboin, I.; Ksouri, M.; Lejay, E.; Wiart, R., *Electrochim.Acta* **1975**, 20, 603  
(b) Epelboin, I; Gabrielli, C.; Keddama, M., in *Comprehensive Treatise of Electrochemistry*, Yeager, E. (Ed.), Vol.9, Plenum Press, New York, 1984, p.1.
- (23) Wacker, A.; Schöll, *Appl.Phys.Lett.* **1991**, 59, 1702.
- (24) Wu, J.C.;Wybourne, M.N.; Berven, C.; Goodnick, S.M.; Smith, D.D., *Appl.Phys.Lett.* **1992**, 61, 2425.
- (25) Niedernostheide, F.-J.; Berner, B.S.; Purwins, H.-G., *Phys.Rev.B* **1992**, 46, 7559

## Figure captions

### Figure 1

Cyclic voltammetry of CO electro-oxidation in the model. (a) Influence of voltage scan rate; (b) Influence of disk rotation rate. The following values for the model parameters were used:  $k_{\text{OH,ads}}=10^{-4} \text{ s}^{-1}$ ,  $k_{\text{OH,des}}=10^5 \text{ s}^{-1}$ ,  $k_r=10^{-5} \text{ s}^{-1}$ ,  $k_{\text{CO,ads}}=10^8 \text{ cm}^3 \text{ mol}^{-1} \text{ s}^{-1}$ ,  $c_{\text{CO,bulk}}=10^{-6} \text{ mol cm}^{-3}$ ,  $D_{\text{CO}}=5 \times 10^{-5} \text{ cm}^2 \text{ s}^{-1}$ ,  $\theta_{\text{OH}}^{\text{max}}=0.333$ ,  $S_{\text{tot}}=2.2 \times 10^{-9} \text{ cm}^{-2}$ ,  $\delta=1.34 \times 10^{-3} \text{ cm}$  (2500 rpm),  $2.23 \times 10^{-3} \text{ cm}$  (900 rpm),  $6.7 \times 10^{-3} \text{ cm}$  (100 rpm).

### Figure 2

S-shaped polarization curve observed for  $\delta=6.7 \times 10^{-3} \text{ cm}$  (100 rpm), other parameter values as in Fig.1. The thin line shows the cyclic voltammetry observed at a low scan rate of 2 mV/s.

### Figure 3

Galvanodynamic scans as obtained from the model for two different current scan rates. Parameter values as in Fig.2.

### Figure 4

Cyclic voltammetry of a Pt(110) RDE in a CO saturated 0.1 M HClO<sub>4</sub> solution. (a) Influence of the voltage scan rate; (b) influence of the disk rotation rate.

### Figure 5

Galvanodynamic scans of a Pt(110) RDE in a CO saturated 0.1 M HClO<sub>4</sub> solution at two different current scan rates (400 rpm). Insert shows the potential fluctuations observed at an applied current density of 0.74 mA/cm<sup>2</sup> (900 rpm).

### Figure 6

Galvanodynamic scans of a Pt(111) RDE in a CO saturated 0.1 M HClO<sub>4</sub> solution at two different current scan rates (2500 rpm). (a) 50 μA/s, (b) 2 μA/s.

Figure 7

Galvanodynamic scans of a Pt(100) RDE in a CO saturated 0.1 M HClO<sub>4</sub> solution at two different current scan rates (400 rpm).

Figure 8

Comparison of the cyclic voltammetry of a Pt(111) RDE in a CO saturated 0.05 M H<sub>2</sub>SO<sub>4</sub> and 0.1 M HClO<sub>4</sub> solution. Scan rate 20 mV/s, rotation rate 900 rpm.

Figure 9

Galvanodynamic scans of a Pt(111) RDE in a CO saturated 0.05 M H<sub>2</sub>SO<sub>4</sub> solution at two different current scan rates (400 rpm): (a) 20 μA/s, (b) 2 μA/s. (c) Potential oscillations observed at a current density of 0.583 mA/cm<sup>2</sup> (400 rpm).